Powder Technology 405 (2022) 117521

Contents lists available at ScienceDirect

Powder Technology

journal homepage: www.elsevier.com/locate/powtec

# Discrete element thermal conductance model for sintered particles

J. Rojek *, R. Kasztelan, R. Tharmaraj

*Institute of Fundamental Technological Research, Polish Academy of Sciences, Pawińskiego 5B,02-106, Warsaw, Poland*

ARTICLE INFO

*Article history:*
Received 14 February 2022
Received in revised form 11 May 2022
Accepted 12 May 2022
Available online 16 May 2022

*Keywords:*
Sintering
Particles
Discrete element method
Thermal conductance
Pipe-network model
Volume conservation
Heat conduction

ABSTRACT

A discrete element thermal conductance model suitable for the modelling of heat flow between sintered particles has been proposed. The model is formulated using the sintering geometry consisting of two spheres connected with a cylindrical neck. The calculation of the neck size is based on the criterion of volume conservation. Therefore the neck obtained is more accurate than that of the popular Coble's model. The thermal conductance is determined for different neck sizes by the finite element simulations of the heat flow in half of the sintering geometry. The numerical results are fitted with a linear relationship which is the basis to determine the equivalent conductance between two sintered particles. The model can be used in the pipenetwork formulation of the discrete element method for simulation of heat conduction problems in powder sintering or in sintered porous materials.



## 1. Introduction

Sintering is a powder consolidation process in which an initially compacted powder is heated and densified by keeping it at an elevated temperature below the melting point. In the initial stage of sintering, cohesive bonds are formed between powder particles (Fig. 1). When the sintering process is continued, the necks between particles grow due to diffusive mass transport. The neck growth leads to a gradual elimination of porosity and macroscopic shrinkage. Sintering is used to obtain fully dense materials (with very low porosity) [21] as well as porous materials [23].

The discrete element method (DEM) has been shown to be a suitable tool to model sintering processes [9,12,14,24]. In the DEM, the powder material is represented by an assembly of spherical particles. Sintering is modelled in the DEM considering mechanical interaction and the relative approach of bonded particles. The DEM sintering models [12,14, 24] are usually based on the two-particle sintering model developed by Coble [3]. Although sintering is a thermomechanical problem thermal effects were usually treated in a simplified way in DEM models of sintering. Simulation of sintering was performed for isothermal conditions [12,24], or a uniform temperature in the sintered material changing according to a prescribed time function was assumed [14]. Conventional sintering is a very slow process, so the assumption of uniform temperature and, as a consequence, neglecting heat transfer between particles is fully justified. Heat conduction between powder particles has been taken into account in DEM models of non-conventional sintering, such as electrically enhanced sintering [27] or selective laser sintering [8]. Termomechanical DEM coupled model has been used in the simulation of high heating rate sintering [22]. The DEM thermal model can also be useful to analyse the thermal or electrical conductivity of partially sintered porous material [18].

An exact treatment of the heat conduction through sintered particles would require a certain discretisation of particles. Finite element discretisation of discrete elements was used to determine the evolution of the effective thermal conductivity of the powder during spark plasma sintering by Zhang and Zavaliangos [26]. Such modelling is, however, computationally very expensive, and its practical use is limited to a small number of particles.

Efficient modelling of heat conduction in the granular material is possible using the so-called thermal pipe-network model in the thermal formulation of the discrete element model [4]. The thermal pipe network model is the lattice type model created by truss thermal elements connecting particle centres. Heat flow in the thermal pipe can be expressed in terms of the average temperatures of connected particles and a certain heat conductance parameter. The thermal pipe-network DEM model has been used to evaluate the effective thermal conductivity of randomly packed granular material by Liang [7]. The network model has been used by Roussel et al. [18] to evaluate the effective electrical conductivity of a sintered porous material. The flow of electricity can be treated in the same way as heat conduction taking advantage of the thermal-electrical analogy [15].

The conductance of the thermal pipes is contributed by the conductance of the particles as well as by the conductance properties of the contact interface between particles. In the case of small Biot numbers

* Corresponding author.
*E-mail addresses:* jrojek@ippt.pan.pl (J. Rojek), rkasztel@ippt.pan.pl (R. Kasztelan), tramakr@ippt.pan.pl (R. Tharmaraj).

https://doi.org/10.1016/j.powtec.2022.117521

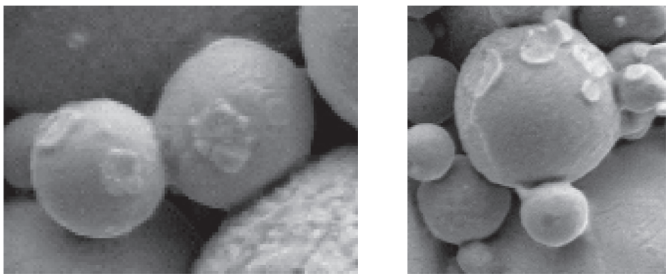


**Fig. 1.** SEM images of bonded particles during sintering – fracture of a material at an early stage sintering: (a) nearly equal size particles, (b) unequal size particles.

characterising the ratio of the conduction resistance within a solid body (particle) to the conduction resistance external to the body, the heat conduction in the particle can be neglected, which means a uniform temperature in the particle can be assumed, and heat exchange between particles is governed by the thermal resistance/conductance of the contact interface and temperature jump at the contact [27]. This assumption is justified for small particles. Uniform temperatures within particles have been assumed in the thermal DEM by many authors, cf. [5,10,17,25]. This assumption has also been used in the thermal part of the DEM thermomechanical model of the high heating rate sintering by Teixeira et al. [22]. The interparticle conductance in the thermal contact model is expressed as a function of the heat transfer coefficient and the actual contact area.

A more general DEM thermal model is one based on the pipe network approach. It can take into account both heat conduction in the particle, and if necessary, it can additionally include a contribution of the contact interface [4,18,25]. The conductance of the thermal pipe can be determined by solving the problem of heat between two contacting particles numerically. The equivalent conductance for two sintered particles with various neck radii was calculated using the finite difference method by Birnboim et al. [2]. Argento and Bouvard [1] calculated the thermal resistance (inverse of the conductance) of two touching deformed spheres of equal size by the finite element method. It has been shown by Birnboim et al. [2] and Argento and Bouvard [1] that the thermal conductance can be approximated by a linear function of the radius of contact/neck area.

Thus, the neck or contact area radius is a parameter controlling heat flow in the thermal pipe as well as in the heat exchange at the contact. Its determination is very important in the evaluation of heat conduction in the discrete element method. When the DEM thermal model is applied to an assembly of loose or mechanically compacted particles, the contact area can be determined using an appropriate mechanical contact model. Gobal and Ravani [6] calculated the radius of the contact area using the Hertzian contact model between two elastic spheres. The contact radius between two sintered particles under compression was evaluated by finite element computation assuming a plastic material model by Semenov et al. [20]. It was shown that the neck radius obtained from the plastic model is more than twice that of the elastic one. Ganeriwala and Zohdi [5], Zohdi [27], and Quintana-Ruiz and Campello [16] calculated the contact area between sintered particles as the intersection area of overlapping spheres. The evolution of the neck radius during sintering can be determined by solving the diffusion problem numerically [19]. Neck radius in the finite difference calculations of two spheres by Birnboim et al. [2] was obtained by the numerical solution of Coble's sintering model for the surface diffusion [3]. A finite difference model was also used to determine the neck growth rate caused by surface diffusion by Matsuda [13]. This is, however, quite an expensive approach and difficult to use in the discrete element method. As an efficient alternative, the model of two-particle sintering proposed by Coble [3], and commonly used in the mechanical discrete element model of powder sintering, e.g. [11], is also used to determine the neck radius in the discrete element thermal models of sintered particles [18] or undergoing sintering [22].

The review presented here shows some inconsistencies of discrete element thermal models of sintered particles. First of all, in many models, the determination of the neck radius is based on oversimplified assumptions. Calculation of the contact surface according to the elastic or elastoplastic contact models, e.g. [6,20], does not correspond to the physical phenomena occurring at the particle contact zone during sintering, i.e. neck growth due to diffusion. Neither is the neck growth treated appropriately in the geometrical considerations employed in [5,16,27]. Coble's analytical formula for the neck radius based on the sintering model and used for instance in [18,22] gives a good assessment of neck size for the initial stage sintering, however as it will be shown in this paper, it overestimates the neck size and the error increases with the neck growth. As a result, the total volume in the system of two particles connected by the neck is not conserved. The neck radius is the main parameter of the conductance models for sintered particles, including the model given by the relationship obtained by Argento and Bouvard [1] and used by Roussel et al. [18]. This model is suitable for the DEM thermal formulation. It is given by a simple linear relationship, and it is based on the analysis of heat conduction in a pair of contacting particles with a varying contact area. Here, it must be noted, however, that in the original calculations, Argento and Bouvard [1] used the geometry of particles deformed plastically under compressive force. The aim of the present work is to establish a new model for the thermal conductance of sintered particles suitable for the discrete element method. An original sintering geometry consisting of two spheres connected with a cylindrical neck will be proposed. Unlike the popular Coble's model, the new geometrical model will satisfy exactly the criterion of volume conservation. Determination of the cylindrical neck size requires the solution of a nonlinear problem. An efficient iterative solution will be proposed. The proposed sintering geometry will be used to perform FE analysis of the heat conduction. The results of the FEM simulations will be used to determine the thermal conductance of the particle–neck–particle neck system as a function of the neck radius. Unlike the relationship obtained by Argento and Bouvard [1], the new model will be based on the FE simulations on the sintering geometry.

The outline of the paper is as follows. Thermal pipe-network formulation of the discrete element method is briefly described in Section 2. The conductance parameter of the thermal pipe is introduced. Evaluation of the equivalent conductance of two contacting particles by a combination of contributions of the particles and the contact area is presented in Section 3. Sintering geometries of Coble's model and the model with a cylindrical neck are defined in Section 4. Calculation of the cylindrical neck radius based on the criterion of mass preservation is presented. The necks calculated in this way are compared with the neck size in Coble's model showing the lack of volume conservation in Coble's model. Thermal conductance of a semisphere with a neck (half of the sintering geometry) is determined for different neck sizes with the finite element simulation in Section 5. The numerical results are approximated with a linear analytical relationship which is the basis for the evaluation of thermal conductance for a pair of sintered particles which is shown in Section 6. Finally, the work is summarised, and conclusions are given.

## 2. Thermal formulation of the discrete element method

The discrete element method for thermal analysis based on the thermal pipe network model [4] employs a system of lumped capacitances $C_i$ concentrated at the particle centres given by

$$C_i = m_i c\,, \tag{1}$$

where $m_i$ is the particle mass and $c$ – the specific heat. The centres of contacting particles are connected with the conducting bars (thermal

pipes). The pipe network model of the heat conduction in the particle system is shown schematically in Fig. 2.

The rate of heat storing in the lumped capacitance should be in balance with the rate heat flow through the pipes and any other contributions of heat transfer. The heat balance equation for the $i$-th particle can be written in the following form:

$$C_i \dot{T}_i = \dot{Q}_i \,, \tag{2}$$

where $T_i$ is the average temperature of the $i$-th particle, and $\dot{Q}_i$ is the resultant heat flow rate (heat flux) including the rate of heat conducted through the pipes $\dot{Q}_{ij}^{cond}$, the rate of internal heat generation (for instance due to Joule heating) $\dot{Q}_i^{int}$, and the rate of heat transfer to the environment due to convection or radiation, $\dot{Q}_i^{conv}$ and $\dot{Q}_i^{rad}$, respectively

$$\dot{Q}_i = \sum_{j=1}^{n_c} \dot{Q}_{ij}^{cond} + \dot{Q}_i^{int} + \dot{Q}_i^{conv} + \dot{Q}_i^{rad} \,. \tag{3}$$

where $n_c$ is the number of particles in contact with the $i$-th particle. The conductive heat flux $\dot{Q}_{ij}$ between particles $i$ and $j$ can be expressed in terms of particle temperatures, $T_i$ and $T_j$, and a certain heat conductance parameter $K_{ij}$

$$\dot{Q}_{ij} = K_{ij}(T_j - T_i) \tag{4}$$

Determination of the heat conductance for sintered particles is the main objective of the present paper. Eq. (2) supplemented with initial conditions (initial particle temperatures) defines the initial value problem. The solution of this problem by an appropriate time integration method yields the evolution of particle temperatures.

## 3. Equivalent conductance of a pair of particles

The equivalent conductance $K_{ij}$ for a pipe connecting particle centres can be obtained by combining contributions of the particles as well as that of the contact interface. Following [4] and taking advantage of the analogy to the electrical resistors connected in series the equivalent thermal resistance $R_{ij}$ can be expressed in terms of the constituent resistances as follows

$$R_{ij} = R_i + R_j + R_c \,, \tag{5}$$

where $R_i$ and $R_j$ are resistances of the pipes representing contributions of the respective particles, and $R_c$ is the contact resistance. If the contribution of the contact interface can be neglected, then

$$R_{ij} = R_i + R_j \,. \tag{6}$$

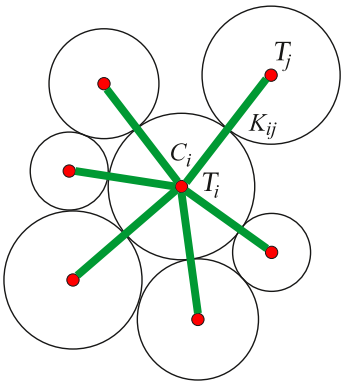


**Fig. 2.** Pipe network model.

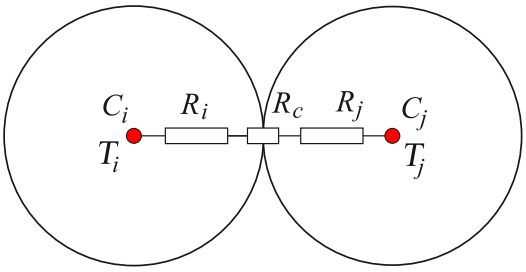


**Fig. 3.** Thermal pipe connecting two particles with a contact interface.

Conductance and resistance are related by the inverse relationship:

$$K_{ij} = \frac{1}{R_{ij}} \,, \quad K_i = \frac{1}{R_i} \,, \quad K_j = \frac{1}{R_j} \,, \quad K_c = \frac{1}{R_c} \,. \tag{7}$$

Thus, the respective formulae for Eqs. (5) and (6) are the following:

$$K_{ij} = \frac{K_i K_j K_c}{K_i K_j + K_j K_c + K_i K_c} \,, \tag{8}$$

$$K_{ij} = \frac{K_i K_j}{K_i + K_j} \,. \tag{9}$$

## 4. Geometrical models of two particle sintering

### 4.1. Coble's model

The geometry assumed by Coble [3] for the two-particle sintering model with shrinkage is shown in Fig. 4. It consists of two spheres of radii $r$ intersecting each other with overlap $h$. The neck of radius $a$ has concave curvature with radius $\rho$. The geometric parameters are linked by the following relationship [3]:

$$\frac{h}{2} = \rho = \frac{a^2}{4r} \tag{10}$$

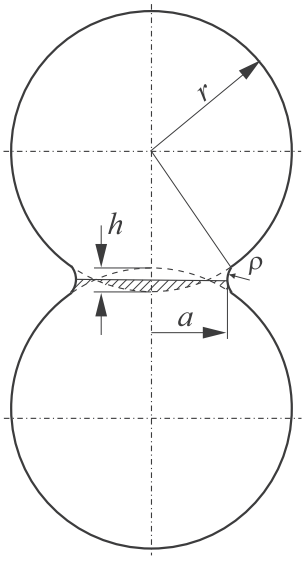


**Fig. 4.** Sintering geometry of two-particle Coble's model.

Thus, for a given overlap $h$ the neck radius $a$ can be obtained as

$$a = \sqrt{2\mathrm{r}\ \mathrm{h}} \tag{11}$$

The model was proposed by Coble for equal-sized particles. It can be adapted for a pair of unequal sized particles with different radii $r_i$ and $r_j$ substituting radius $r$ in Eq. (11) with the effective radius $r^*$, cf. [12]:

$$r^* = \frac{2r_i r_j}{r_i + r_j} \tag{12}$$

It should be remarked that Coble proposed this model for initial sintering [3]. It is commonly accepted that it is valid for values of $a/r$ ratio up to 0.6 [12], however in practice, in numerical simulations, it can be used with some corrections for larger ratios $a/r$ [18]. Coble's model is based on approximate geometrical relationships. Actually, equalities in Eq. (10) are approximate. As it will be shown further, Eq. (10) overestimates the neck size, and therefore the volume of the particle-neck-particle system is not conserved. A simplified geometry with the cylindrical neck will be proposed below. This simplification will allow calculation of the neck based on the volume conservation criterion.

### 4.2. Model with a cylindrical neck for equal-sized particles

We assume that two spherical particles of radii $r$ undergoing sintering are connected with a neck which can be idealised as a cylinder of height $h_n$ and radius $a$. The assumed sintering geometry is shown in Fig. 5. The distance between the particle centres $d$ is given as

$$d = 2r - h \tag{13}$$

where $h$ is the overlap of two spheres. The aim is to determine the neck radius $a$ for given particle radii $r$ and overlap $h$ based on the criterion of volume conservation. We observe that the volume of cylindrical neck $V_{cyl}$ must be equal to twice the volume $V_{cap}$ of the spherical cap with the radius of the base equal $a$ and the height $h_c$ (Fig. 5):

$$V_{\mathrm{cyl}} = 2V_{\mathrm{cap}} \tag{14}$$

which after applying the formulae for the volumes of the cylinder and caps can be rewritten as follows:

$$\pi a^2 h_n = 2\left(\pi h_c^2 r - \frac{\pi}{3}h_c^3\right) \tag{15}$$

Eq. (15) contains three unknowns: $a$, $h_n$ and $h_c$. The set of equations will be completed with two geometrical relationships:

$$h_n = 2h_c - h \tag{16}$$

$$r^2 = a^2 + (r - h_c)^2 \tag{17}$$

Eliminating the unknowns $a$ and $h_n$ from the set of Eqs. (15)–(17) the following quadratic equation can be obtained for $h_c$:

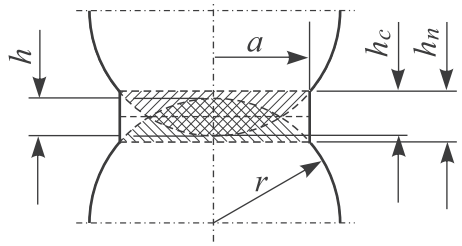


**Fig. 5.** Two equal particles connected by the neck.

$$4h_c^2 - 3(2r + h)h_c + 6\mathrm{rh} = 0\,. \tag{18}$$

The only physically meaningful solution of the quadratic Eq. (18) is the following:

$$h_c = \frac{3(2r + h) - \sqrt{9(2r + h)^2 - 96\mathrm{rh}}}{8}\,. \tag{19}$$

Eq. (17) can be rewritten as

$$a = \sqrt{2rh_c - h_c^2}\,. \tag{20}$$

Substituting expression (19) into Eq. (20), we obtain the explicit expression for the neck radius $a$ based on the criterion of the volume conservation. The neck radius determined from Eqs. (19) and (20) normalised with respect to the particle radius $r$ is plotted in Fig. 6 in comparison with the normalised neck radius according to Coble's model given by Eq. (11) as a function of the normalised overlap. It can be clearly seen that Coble's model overestimates the neck size. The per cent error of the Coble's neck radius with respect to the neck radius based on the volume preservation criterion is plotted as a function of the normalised neck radius in Fig. 7.

### 4.3. Model with a cylindrical neck for unequal-sized particles

Let us consider a pair of spherical particles of radii $r_i$ and $r_j$ ($r_i < r_j$) undergoing sintering (Fig. 8). The distance between the particle centres $d$ is known, so the particle overlap $h$ ($h > 0$) is given by

$$h = r_i + r_j - d\,. \tag{21}$$

We assume the sintering neck connecting particles can be idealised as a cylinder of height $h_n$ and radius $a$. The neck radius cannot be larger than the radius of the smaller particle: $a \le r_i$.

The aim is to determine the neck radius $a$ satisfying the requirement of volume preservation. The volume is preserved if the volume of cylindrical neck $V_{cyl}$ is equal to the volumes $V_{cap(i)}$ and $V_{cap(j)}$ of the spherical caps being the intersections of the cylindrical neck and the particles (Fig. 8):

$$V_{\mathrm{cyl}} = V_{\mathrm{cap}(i)} + V_{\mathrm{cap}(j)} \tag{22}$$

The radius of the bases of the caps is equal $a$, and their heights are $h_{ci}$ and $h_{cj}$. Substituting the formulae for the volumes of the cylinder and spherical caps into Eq. (22) we obtain

$$\pi a^2 h_n = \pi h_{\mathrm{ci}}^2 r - \frac{\pi}{3}h_{\mathrm{ci}}^3 + \pi h_{\mathrm{cj}}^2 r - \frac{\pi}{3}h_{\mathrm{cj}}^3 \tag{23}$$

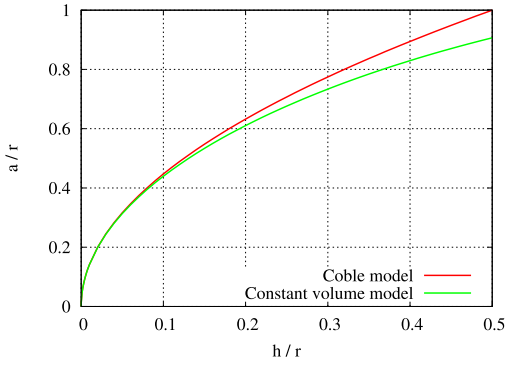


**Fig. 6.** Neck radius as a function of overlap for the same size particles.

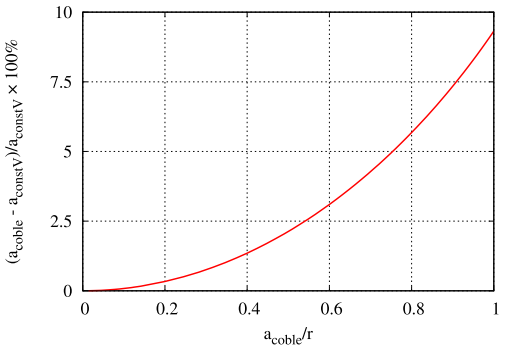


**Fig. 7.** Percent error of the neck radius according to the Coble's model as a function of the normalised neck radius.

Eq. (23) contains four unknowns: $h_{ci}$, $h_{cj}$, $a$ and $h_n$. The set of equations will be completed with three geometrical relationships:

$$h_n = h_{\mathrm{ci}} + h_{\mathrm{cj}} - h \tag{24}$$

$$r_i^2 = a^2 + (r_i - h_{\mathrm{ci}})^2 \tag{25}$$

$$r_j^2 = a^2 + (r_j - h_{\mathrm{cj}})^2 \tag{26}$$

It would be difficult to obtain a closed-form solution of the problem defined by the set of Eqs. (23)–(26). We will present a numerical solution to this problem.

Let us rewrite Eq. (23) as

$$Z = 3a^2 h_n - h_{\mathrm{cj}}^2(3r_j - h_{\mathrm{cj}}) - h_{\mathrm{ci}}^2(3r_i - h_{\mathrm{ci}}) = 0 \tag{27}$$

and Eqs. (25) and (26) in the following form:

$$h_{\mathrm{ci}} = r_i - \sqrt{r_i^2 - a^2} \tag{28}$$

$$h_{\mathrm{cj}} = r_j - \sqrt{r_j^2 - a^2} \tag{29}$$

It can be easily noted that $Z$ introduced in Eq. (27) is an implicit function of $a$:

$$Z = Z(a, h_{\mathrm{ci}}(a), h_{\mathrm{cj}}(a), h_n(h_{\mathrm{ci}}(a), h_{\mathrm{cj}}(a))) \tag{30}$$

where $h_{ci}(a)$, $h_{cj}(a)$, and $h_n(h_{ci}(a), h_{cj}(a))$ are defined by Eqs. (28), (29) and (24), respectively. Function $Z$ for $r_i = 1$ mm, $r_j = 3$ mm, and $h = 0.2$ mm has been calculated in the interval $a = [0, r_i]$ and plotted in Fig. 9a).

The nonlinear Eq. (27) can be solved using a suitable numerical method, such as the bisection or Newton's method. Newton's method requires evaluation of the derivative $Z'(a)$ which can be calculated using the chain rule for implicit differentiation:

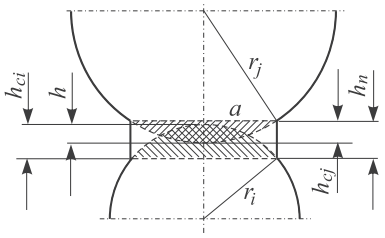


**Fig. 8.** Two particles of different size connected by the neck.

$$Z'(a) = \frac{\mathrm{d}Z}{\mathrm{d}a} = \frac{\partial Z}{\partial a} + \frac{\partial Z}{\partial h_{\mathrm{ci}}}\frac{\mathrm{d}h_{\mathrm{ci}}}{\mathrm{d}a} + \frac{\partial Z}{\partial h_{\mathrm{cj}}}\frac{\mathrm{d}h_{\mathrm{cj}}}{\mathrm{d}a} + \frac{\partial Z}{\partial h_n}\left(\frac{\partial h_n}{\partial h_{\mathrm{ci}}}\frac{\mathrm{d}h_{\mathrm{ci}}}{\mathrm{d}a} + \frac{\partial h_n}{\partial h_{\mathrm{cj}}}\frac{\mathrm{d}h_{\mathrm{cj}}}{\mathrm{d}a}\right) \tag{31}$$

The successive iterations in the Newton's method can be presented generally as

$$a_i = a_{i-1} - \frac{Z(a_{i-1})}{Z'(a_{i-1})} \tag{32}$$

The Coble's radius is a good starting point for the Newton's method:

$$a_0 = a_{\mathrm{Coble}} \tag{33}$$

The Newton's solution with the Coble's neck radius $a_{\mathrm{Coble}}$ taken as $a_0$ is presented graphically in Fig. 9b). Since the difference is not so large even the first iteration

$$a_1 = a_{\mathrm{Coble}} - \frac{Z(a_{\mathrm{Coble}})}{Z'(a_{\mathrm{Coble}})} \tag{34}$$

gives very good approximation of the neck radius $a$. In the case presented in Fig. 9, the value of the neck radius obtained by Newton's method with 6-digit accuracy is $a = 0.741466$ mm, the Coble's solution is 0.774597 mm (error 4.47%), and the first iteration gives $a_1 = 0.745039$ mm, which gives an error of 0.48%.

The neck radii for different particle size ratio $r_j/r_i$ obtained by the Newton's method are plotted in Fig. 10. The difference between the neck radii according to the Coble's model and those obtained from the volume preservation criterion is illustrated in Fig. 11 by the per cent error.

## 5. Thermal conductance of a semisphere with a neck

The effective conductance $K_{ij}$ a thermal pipe connecting the centres of a pair of sintered particles will be evaluated by combining contributions (conductances $K_i$ and $K_j$) of the particles according to formulae presented in Section 3. The conductance $K_i$ in a pair of equal size particles will be determined for considering heat conduction through the half of the sintering geometry shown in Fig. 5. Definition of geometry and boundary conditions for the thermal problem is presented in Fig. 12. The segment of a sphere of radius $r = 10$ mm with the bases of radii $r$ and $a$ is combined with the cylinder of radius $a$ and height $h_n/2$. A number of cases with different $a$ ($0 < a < r$) corresponding to different overlaps $h$ have been analysed. The neck radius $a$ and height $h_n$ have been determined using Eqs. (19) and (20).

The steady-state heat conduction problem has been analysed. The insulation of the lateral surface and prescribed temperatures 10°C at the top surface and 0°C at the bottom surface have been assumed as boundary conditions. Thermal properties of copper have been assumed with the thermal conductivity $\kappa = 394$ W/(m·°C). The geometry has been discretised with four-node axisymmetric quadrilateral finite elements. The heat conduction analysis has been performed using the Abaqus finite element program. The results for the four analysed cases are presented in Fig. 13 in the form of temperature distribution. It can be observed that the necks affect the temperature field. Higher temperature gradients across the necks, especially close to the intersection of the cylindrical and spherical surfaces, can be observed. According to Fourier's thermal conductance law, the higher temperature gradient $\nabla T$ the higher heat flux density $q$ is:

$$q = -\kappa \nabla T\,. \tag{35}$$

Fig. 14 shows the distribution of the magnitude of the heat flux density $q$. Higher thermal fluxes can be noticed in the necks, and their concentration close to the neck–particle connections is manifested. This effect is more pronounced for smaller neck sizes.

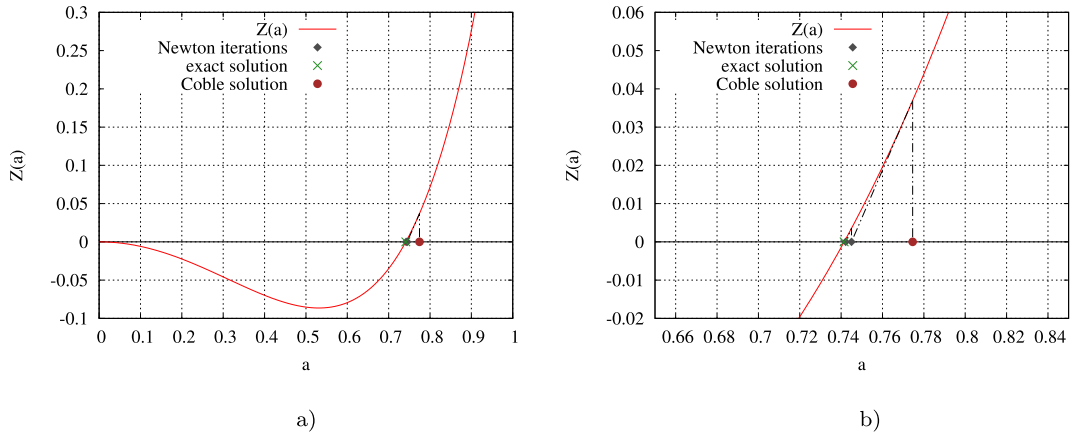


**Fig. 9.** Function $Z$ vs. neck radius $a$ for $r_i = 1$ mm, $r_j$=3 mm, and $h = 0.2$ mm: (a) overall graph, (b) zoom.

The simulation results have been used to determine the equivalent conductance of the semisphere with the cylindrical neck. The equivalent conductance $K_i$ of the sintering geometry analysed here can be determined as follows

$$K_i = \frac{\dot{Q}}{\Delta T} \tag{36}$$

where $\Delta T$ is the temperature difference between the top and bottom, and $\dot{Q}$ is the heat flow rate measured in J/s through any horizontal cross-section of the analysed geometry. The heat flow rate can be easily calculated by summing its nodal values at the top or bottom surface, which are evaluated in the FEM calculations

$$\dot{Q} = \sum \dot{Q}_i \tag{37}$$

In order to ensure sufficient accuracy of the convergence of the solution with mesh refinement has been studied for all the cases. Convergence of the values of the equivalent conductance with the increasing number of elements across the neck height for the case $h/r = 0.08$ has been plotted in Fig. 15. It is shown that with the increase of the number of elements (decrease of the element size) a nearly steady value of the equivalent conductance is obtained. The equivalent conductance $K_i$ has been evaluated in this way for all the cases and normalised with respect to the conductance $K_{cyl}$ of the cylinder of radius $r$ and height $r$. The conductance of the cylinder $K_{cyl}$ has been obtained as

$$K_{\mathrm{cyl}} = \kappa \frac{A_{\mathrm{cyl}}}{L_{\mathrm{cyl}}} \tag{38}$$

where $\kappa$ is the conductivity of the material, $L_{cyl}$ is the cylinder height, $L_{cyl} = r$, and $A_{cyl}$ is the cylinder cross-section area

$$A_{\mathrm{cyl}} = \pi r^2 . \tag{39}$$

The ratio $K_i/K_{cyl}$ is plotted as a function of the cylindrical neck radius normalised with respect to the particle radius $r$ in Fig. 16.

It can be seen in this figure that the relationship between $K_i/K_{cyl}$ and $a/r$ up to nearly $a/r = 0.7$ has a linear character. The numerical results can be fitted by the linear approximation

$$\frac{K}{K_{\mathrm{cyl}}} = 1.064 \frac{a}{r} \tag{40}$$

The results presented here are consistent with the results obtained by Argento and Bouvard [1] who calculated the thermal resistance (inverse of the conductance) of two touching deformed spheres of equal size by the finite element method. The numerical results for different stages of particle deformation were fitted with the analytical realtionship:

$$\frac{R_{\mathrm{ij}}}{R_{\mathrm{cyl}}} = 0.899 \left(\frac{a}{r}\right)^{-1} \tag{41}$$

where $R_{ij} = 1/K_{ij}$ is the thermal resistance of two deformed spheres in contact, $r$ – the sphere radius, $a$ – the contact radius, and $R_{\mathrm{cyl}}$ – the thermal resistance of a cylinder of radius $r$ and height $2r$. The relationship (41) can be rewritten in terms of conductances as follows

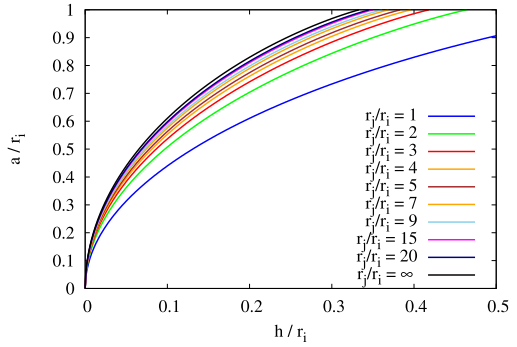


**Fig. 10.** Neck radius as a function of overlap for different size particles.

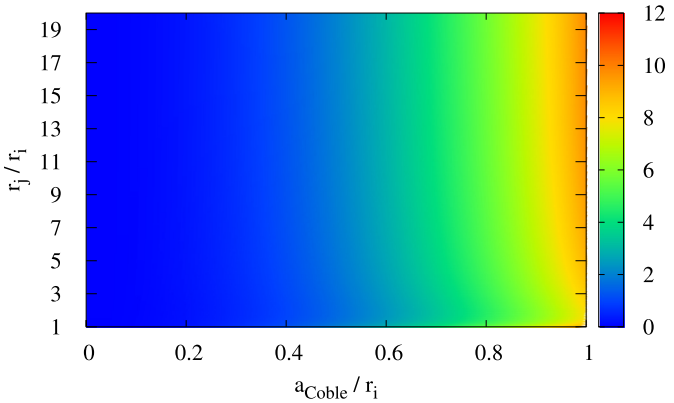


**Fig. 11.** Percent error of the Couble radius with respect to volume preservation solution.

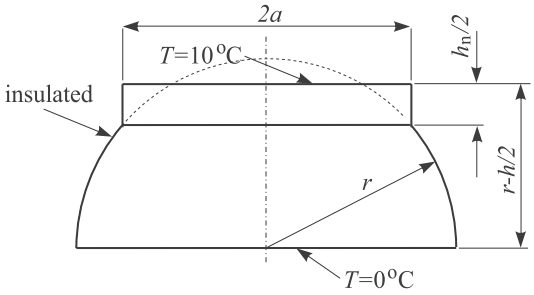


**Fig. 12.** Semisphere with a neck – definition of geometry and thermal boundary conditions.

$$\frac{K}{K_{\text{cyl}}} = \frac{1}{0.899}\frac{a}{r} = 1.112\frac{a}{r} \tag{42}$$

The difference of the slope obtained in our simulations with respect to that obtained by Argento and Bouvard [1] is around 3%. It must be remembered that the geometry used in both studies was different. Argento and Bouvard [1] used the deformed configuration of two spheres under compression, and here the idealised sintering geometry has been used.

## 6. Determination of the equivalent conductance of a pair of bonded particles

The linear relationship (40) plotted in Fig. (16) can be used to determine the conductance of the thermal pipe representing two sintered particles. In order to simplify further calculations let us substitute Eqs. (38) and (39) into Eq. (40). Then the conductance $K$ can be obtained as follows:

$$K = 1.064\frac{a}{r}K_{\text{cyl}} = 1.064\frac{a}{r}\kappa\frac{A_{\text{cyl}}}{L_{\text{cyl}}} = 1.064\frac{a}{r}\kappa\frac{\pi r^2}{r} = 1.064\kappa\pi a \tag{43}$$

It is interesting to observe that according to Eq. (43) the conductance $K$ does not depend explicitly on $r$. This means that different size particles connected with a neck of radius $a$ have equal conductances.

The use of Eq. (40) or Eq. (43) for equal size particles does not need any additional justification since simulations in Section 5 have been performed for the sintering geometry of equal size particles. Validity of the relationships (40) as well as (43) will be checked performing additional finite element simulation. Let us consider two sintered particles of radii $r_i$ and $r_j$ made of material with thermal conductivity $\kappa$, and the distance between the centres $d_{ij}$. The procedure to determine the equivalent conductance $K_{ij}$ of the conisdered pair of particles would be the following:

1 The overlap $h$ is determined from Eq. (21) as

$$h = r_i + r_j - d \tag{44}$$

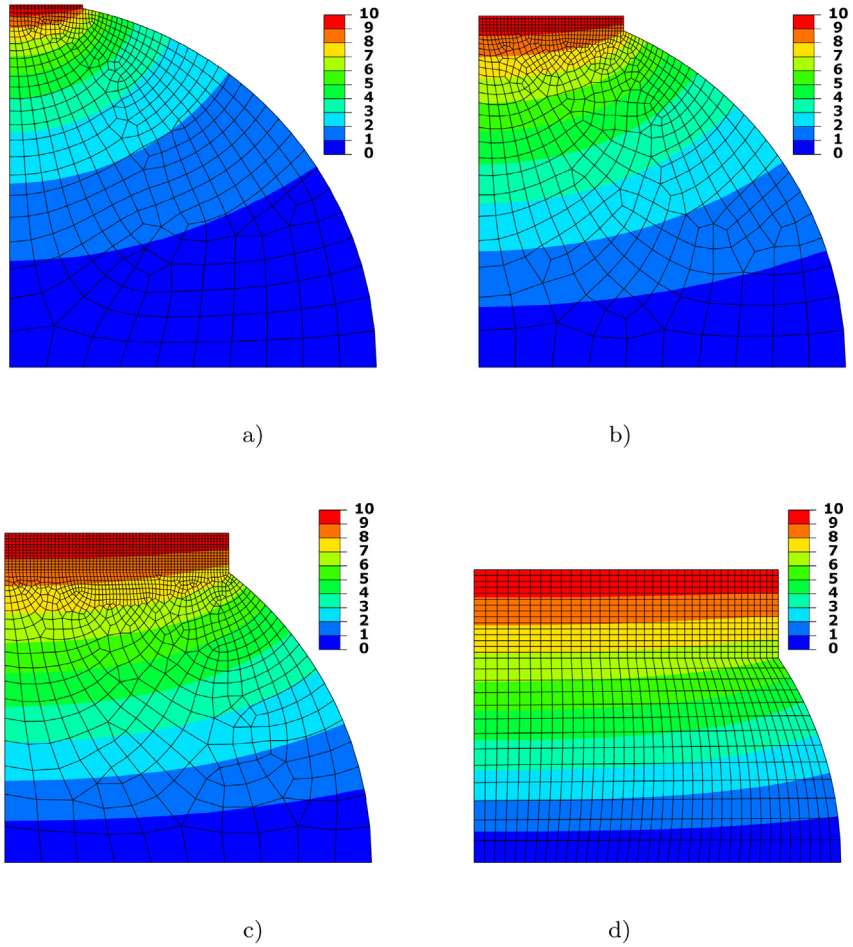


**Fig. 13.** Temperature (in °C) distribution for different neck sizes: (a) $h/r = 0.02$, $a/r = 0.19934$, (b) $h/r = 0.08$, $a/r = 0.3946$, (c) $h/r = 0.2$, $a/r = 0.610573$, (d) $h/r = 0.4$, $a/r = 0.829653$.

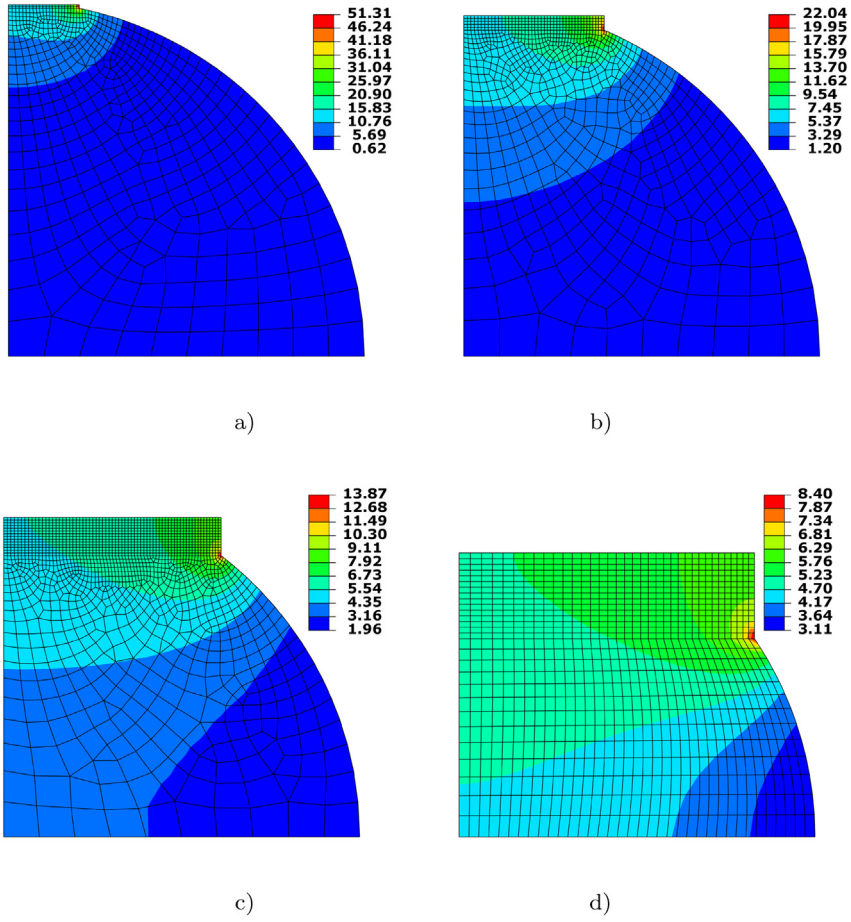


**Fig. 14.** Distribution of the magnitude of heat flux (in W/m$^2$) for different neck sizes: (a) $h/r = 0.02$, $a/r = 0.19934$, (b) $h/r = 0.08$, $a/r = 0.3946$, (c) $h/r = 0.2$, $a/r = 0.610573$, (d) $h/r = 0.4$, $a/r = 0.829653$.

2 If $h > 0$ the neck radius $a$ is calculated: (i) using Eqs. (19) and (20) if $r_i = r_j$, (ii) using Newton's solution of Eq. (27) if $r_i \neq r_j$
3 Conductances $K_i$ and $K_j$ of the parts of the sintering geometry associated with each semisphere are calculated from Eq. (43).
4 Conductance $K_{ij}$ of the thermal pipe connecting two particles is calculated from Eq. (9). Taking into account that according to Eq. (43) $K_i = K_j$ Eq. (9) yields

$$K_{ij} = \frac{K_i}{2} = \frac{K_j}{2}. \tag{45}$$

Let us apply the above procedure to two copper particles of radii $r_i = 1$ mm and $r_j = 3$ mm with overlap $h = 0.06$ mm. The copper thermal

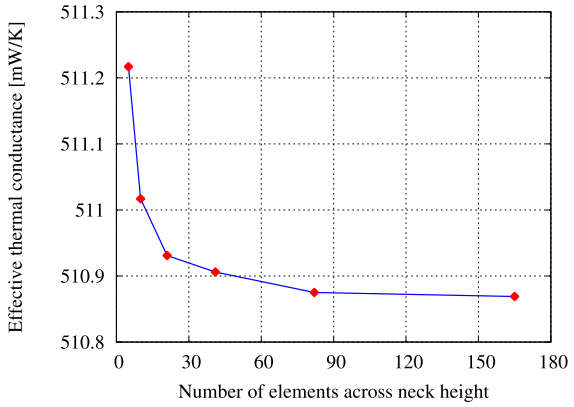


**Fig. 15.** Convergence of the solution with mesh refinement ($h/r = 0.08$, $a/r = 0.3946$).

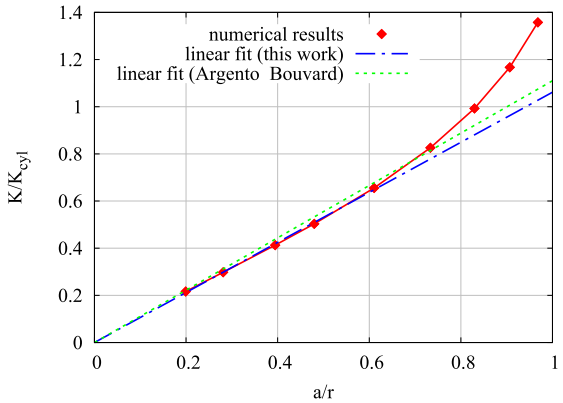


**Fig. 16.** Conductance of semispheres with necks as a function of neck radius.

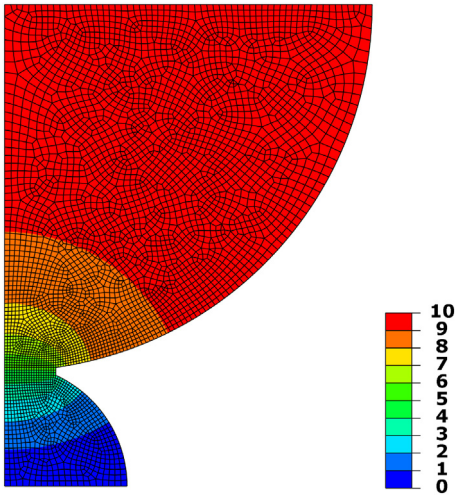


**Fig. 17.** Temperature (in °C) distribution in the system of two different size particles, $r_j/r_i = 3$.

conductivity $\kappa = 394$ W/(m·K) is taken. The neck radius obtained by Newton's method with 6-digit accuracy is $a = 0.419186$ mm. The conductances $K_i$ and $K_j$ are calculated from Eq. (43) as:

$$K_i = K_j = 1.064 \cdot 394 \cdot \pi \cdot 0.419186 \cdot 10^{-3} \text{ W/K} = 0.55207 \text{ W/K}$$

The equivalent conductance for the pair of particles is given by Eq. (45)

$$K_{ij} = K_i/2 = 0.276035 \text{ W/K}$$

Now, the equivalent problem will be determined numerically. The methodology described in Section 5 will be applied to the sintering geometry of unequal size particles shown in Fig. 8 taking $r_i = 1$ mm, $r_j = 3$ mm, $h = 0.06$ mm $a = 0.419186$ mm. The same value of thermal conductivity as above $\kappa = 394$ W/(m·K) is assumed. The steady-state heat flow is analysed for prescribed prescribed temperatures 10°C at the top surface and 0°C at the bottom surface and the isolated lateral surface as boundary conditions. The problem has been analysed as axisymmetric. The geometry has been discretised nonuniformly with quadrilateral axisymmetric finite elements. The mesh with the distribution of temperature is shown in Fig. 17. It is interesting to observe that half of the temperature difference is at the neck, this means that the drop of temperature in both semispheres is equal, so their conductances/resistances are equal as predicted by Eq. (43).

The equivalent conductance $K_{ij}$ of the sintering geometry analysed here has been obtained using Eq. (36). The convergence study with a mesh refinement has been performed. The converged solution has given the equivalent conductance $K_{ij} = 0.278033$ W/K, which agrees very well with the value 0.276035 W/K calculated from the linear relationship (43).

## 7. Conclusions

A new model to determine the conductance of the thermal pipe representing heat flow between sintered particles has been proposed. Unlike the geometry of Coble's model, the sintering geometry of the new model ensures volume conservation. The neck size can be evaluated efficiently using Newton's solution with Coble's neck radius as the starting point. A linear relationship has been established between the conductance and the neck radius in a broad range of neck radius (up to nearly 0.7 of the smaller particle radius). The neck radius is the main parameter controlling heat flow. Therefore, the accuracy of the neck radius is important in the determination of thermal conductance. The thermal conductance model presented in this paper should have the same range of application as Coble's sintering model, i.e. it should be valid for initial stage sintering. The model can be used in the pipe-network formulation of the discrete element method for the simulation of heat conduction problems in powder undergoing sintering or in partially sintered porous materials.

## Declaration of Competing Interest

The author declare that they have no known competing financial interests or personal relationships that could have appeared to influence the ork reported in this paper.

## Acknowledgements

The authors acknowledge the financial support of the National Science Centre, Poland, within research project no. 2019/35/B/ST8/03158.

## References

[1] C. Argento, D. Bouvard, Modeling the effective thermal conductivity of random packing of spheres through densification, Int. J. Heat Mass Trans. 39 (7) (1996) 1343–1350.
[2] A. Birnboim, T. Olorunyolemi, Y. Carmel, Calculating the thermal conductivity of heated powder compacts, J. Am. Ceram. Soc. 84 (2001) 1315–1320.
[3] R.L. Coble, Initial sintering of alumina and hematite, J. Am. Ceram. Soc. 41 (1958) 55–62.
[4] Y.T. Feng, K. Han, D.R.J. Owen, Discrete thermal element modelling of heat conduction in particle systems: Pipe-network model and transient analysis, Powder Technol. 193 (2009) 248–256.
[5] R. Ganeriwala, T.I. Zohdi, A coupled discrete element-finite difference model of selective laser sintering, Gran. Matt. 18 (2016) 21.
[6] A. Gobal, B. Ravani, An adaptive discrete element method for physical modeling of the selective laser sintering process, Appl. Mech. Mater. 869 (2017) 69–84.
[7] Y. Liang, Expression for effective thermal conductivity of randomly packed granular material, Int. J. Heat Mass Trans. 90 (2015) 1105–1108.
[8] X. Liu, Numerical Modeling and Simulation of Selective Laser Sintering in Polymer Powder Bed. PhD thesis, Universite de Lyon, Lyon, France, 2018.
[9] S. Luding, K. Manetsberger, J. Müllers, A discrete model for long time sintering, J. Mech. Phys. Sol. 53 (2005) 455–491.
[10] F.P. Di Maio, A. Di Renzo, D. Trevisan, Comparison of heat transfer models in DEM-CFD simulations of fluidized beds with an immersed probe, Powder Technol. 193 (2009) 257–265.
[11] C.L. Martin, H. Camacho-Montes, L. Olmos, D. Bouvard, R.K. Bordia, Evolution of defects during sintering: discrete element simulations, J. Am. Ceram. Soc. 92 (7) (2009) 1435–1441.
[12] C.L. Martin, L.C.R. Schneider, L. Olmos, D. Bouvard, Discrete element modeling of metallic powder sintering, Scr. Mater. 55 (2006) 425–428.
[13] T. Matsuda, Development of a DEM taking account of neck increments caused by surface diffusion for sintering and application to analysis of the initial stage of sintering, Comput. Mater. Sci. 196 (2021) 110525.
[14] S. Nosewicz, J. Rojek, K. Pietrzak, M. Chmielewski, Viscoelastic discrete element model of powder sintering, Powder Technol. 246 (2013) 157–168.
[15] H. Park, Dynamic Thermal Modeling of Electrical Appliances for Energy Management of Low Energy Buildings, Yeungnam University, Gyeongsan, South Korea, 2014 PhD thesis.
[16] O.D. Quintana-Ruiz, M.B. Campello, A thermo-mechanical formulation for the modeling of discrete particle systems. In Proceedings of the XL Ibero-Latin-American Congress on Computational Methods in Engineering, ABMEC, Natal/RN, Brazil, 2019.
[17] J. Rojek, Discrete element thermomechanical modelling of rock cutting with valuation of tool wear, Comput. Part. Mech. 1 (2014) 71–84.
[18] D. Roussel, A. Lichtner, D. Jauffres, R.K. Bordia, C.L. Martin, Effective transport properties of 3D multi-component microstructures with interface resistance, Comput. Mater. Sci. 96 (2015) 277–283.
[19] A.S. Semenov, J. Trapp, M. Nöthe, O. Eberhardt, B. Kieback, T. Wallmersperger, Thermo-electro-mechanical modeling of spark plasma sintering processes accounting for grain boundary difusion and surface difusion, Comput. Mech. 67 (2021) 1395–1407.
[20] A.S. Semenov, J. Trapp, M. Nöthe, O. Eberhardt, T. Wallmersperger, B. Kieback, Thermo-electro-mechanical modeling, simulation and experiments of field-assisted sintering, J. Mater. Sci. 54 (2019) 10764–10783.
[21] M.V. Sundaram, Processing Methods for Reaching Full Density Powder Metallurgical Materials. Licentiate Thesis, Chalmers University of Technology, Gothenburg, Sweden, 2017.
[22] M.H. Paiva Teixeira, V. Skorych, R. Janssen, S.Y. Gomez Gonzalez, A. De Noni, J.B. Rodrigues Neto, D. Hotza, M. Dosta, High heating rate sintering and microstructural evolution assessment using the discrete element method, Open Cerm. 8 (2021) 100182.
[23] I. Vida-Smiti, Sintered sheets with high porosity. Structure, properties, processing, Annal. Univer. Mech. Eng. 13 (2011) 173–188.

[24] A. Wonisch, T. Kraft, M. Moseler, H. Riedel, Effect of different particle size distributions on solid-state sintering: a microscopic simulation approach, J. Am. Ceram. Soc. 92 (2009) 1428–1434.
[25] H. Xin, W. Ching Sun, J. Fish, Discrete element simulations of powder-bed sintering-based additive manufacturing, Int. J. Mech. Sci. 149 (2018) 373–392.
[26] J. Zhang, A. Zavaliangos, Discrete finite-element simulation of thermoelectric phenomena in spark plasma sintering, J. Electron. Mater. 40 (2011) 873–879.
[27] T. Zohdi, A direct particle-based computational framework for electrically enhanced thermo-mechanical sintering of powdered materials, Mathemat. Mech. Sol. 19 (2014) 93–113.